

Optical Properties of an Ionic Crystal Slab*

RONALD FUCHS, K. L. KLIEWER, AND W. J. PARDEE†

Institute for Atomic Research and Department of Physics, Iowa State University, Ames, Iowa

(Received 14 April 1966)

The theory of the optical properties of an ionic crystal slab is formulated to exhibit explicitly the relation between the optical properties and the virtual modes of the slab. It is shown that the absorption spectrum can be completely understood from the properties of the virtual modes. Expressions for the contribution of a single virtual mode to absorption, reflection, and transmission are compared with exact calculations for LiF. The total width of an absorption peak is shown to be expressible as the sum of a radiative width and a width due to lattice anharmonicities.

I. INTRODUCTION

FROM the point of view of Maxwell's equations, the problem of the optical properties of an ionic crystal slab is understood completely. Knowing the dielectric constant $\epsilon(\omega)$, which describes the response of the material to a long-wave perturbing field, the calculation of the optical properties is straightforward.

If, however, we wish to adopt the point of view that the absorption of photons should be related to the excitation of the normal modes of the slab, the situation is much less clear. Using a weak-coupling approach, we would regard phonons and photons as separate entities coupled by an $\mathbf{E} \cdot \mathbf{P}$ interaction; \mathbf{E} is the electric field of the photons and \mathbf{P} is the polarization due to the phonons. The phonons appropriate to this approach are those obtained with the interaction with transverse photons turned off, or, in other words, neglecting retardation of the Coulomb forces. This calculation was made by the authors¹ and gave phonon frequencies $\omega = \omega(k_x)$, where k_x is the wave-vector component parallel to the slab. If a photon with an angle of incidence θ is absorbed, creating a phonon, the energy $\hbar\omega$ and k_x are conserved. The absorption frequencies would therefore be determined by the intersection of the phonon dispersion curves $\omega = \omega(k_x)$ and the photon line $\omega = kc$ or $\omega = k_x c / \sin\theta$. The only intersections occur at ω_T and ω_L for the sinusoidal modes and at two frequencies between ω_T and ω_L for the surface modes (ω_T and ω_L are the usual transverse and longitudinal optical frequencies in an infinite crystal).

This result is completely incorrect. Although it is true that absorption peaks sometimes occur at ω_T and ω_L , distinct peaks are not found between ω_T and ω_L .² Also, peaks which do occur below ω_T are not explained.

The error in the above approach is that the coupling between phonons and photons is strong, not weak, and should be included from the beginning by taking account of retardation of the Coulomb forces. The true normal

modes involve mixed excitations, the polaritons, and fall into two classes: nonradiative and radiative.^{3,4} Since the nonradiative solutions and the optical properties are unrelated, the optical properties must be described in terms of the radiative solutions, i.e., the virtual modes.⁴ In this paper we show how such a description can be made. We arrive at a point of view in which it is meaningless to think of a process such as the absorption of a photon accompanied by creation of a phonon, since phonons and photons are bound together into a single entity.

II. OPTICAL PROPERTIES OF A SLAB

Although the derivation of the transmission, reflection, and absorption coefficients of a slab is a standard exercise in electromagnetic theory and appears in many textbooks,⁵ a somewhat different derivation is presented here in order to emphasize the relation between these properties and the virtual modes. There is an important difference between the fields involved in an optical experiment and the fields in the virtual modes: Each component of the field in a virtual mode has either even or odd parity about the center of the slab, whereas in an optical experiment, in which light is incident from one side of the slab only, there exists no definite parity. Therefore, a description of the optical properties in terms of the virtual modes involves mixing modes of different parities. This leads to the possibility of interference between modes of different parity and has important consequences in the detailed interpretation of the optical properties.

P Polarization

We imagine an optical experiment performed by letting light be incident on both sides of the slab, choosing the phases so that the fields have definite parity. Using the coordinate system shown in Fig. 1 of II,⁴ we write $\mathbf{E}(\mathbf{r}, t) = \mathbf{E}(z)e^{i(k_x x - \omega t)}$ and let $\beta_0 = (\omega^2/c^2 - k_x^2)^{1/2}$. Then the component $E_x(z)$ outside

* Work was performed in the Ames Laboratory of the U. S. Atomic Energy Commission. Contribution No. 1879.

† Now at Department of Physics, University of Illinois, Urbana, Illinois.

¹ R. Fuchs and K. L. Kliewer, Phys. Rev. **140**, A2076 (1965).

² Peaks in this frequency range due to many-phonon processes are unrelated to this discussion.

³ K. L. Kliewer and R. Fuchs, Phys. Rev. **144**, 495 (1966).

⁴ K. L. Kliewer and R. Fuchs, preceding paper, Phys. Rev. **150**, 573 (1966), to be referred to subsequently as II.

⁵ J. A. Stratton, *Electromagnetic Theory* (McGraw-Hill Book Company, Inc., New York, 1941), Chap. 9.

the slab is of the form

$$\begin{aligned} E_z^{(1)}(z) &= e^{-i\beta_0 z} + P_1 e^{i\beta_0 z}, & z > a \\ &= e^{i\beta_0 z} + P_1 e^{-i\beta_0 z}, & z < -a \end{aligned} \quad (1)$$

for even parity [$E_z(z) = E_z(-z)$], and

$$\begin{aligned} E_z^{(2)}(z) &= e^{-i\beta_0 z} + P_2 e^{i\beta_0 z}, & z > a \\ &= -(e^{i\beta_0 z} + P_2 e^{-i\beta_0 z}), & z < -a \end{aligned} \quad (2)$$

for odd parity [$E_z(z) = -E_z(-z)$]. The first terms in Eqs. (1) and (2) represent waves incident on the slab, and the factors P_1 and P_2 are complex numbers which permit an arbitrary choice of the amplitude and phase of the waves leaving the slab. Adding (1) and (2), we find

$$\begin{aligned} E_z(z) &= 2e^{-i\beta_0 z} + (P_1 + P_2)e^{i\beta_0 z}, & z > a \\ &= (P_1 - P_2)e^{-i\beta_0 z}, & z < -a, \end{aligned} \quad (3)$$

which describes the asymmetric optical experiment; waves incident on the slab from the $+z$ direction only. Since we are assuming P polarization (E in the plane of incidence, the x - z plane), $E_y = H_x = H_z = 0$ and

$$\begin{aligned} E_x(z) &= -\frac{1}{ik_x} \frac{dE_z(z)}{dz} \\ &= (\beta_0/k_x)[2e^{-i\beta_0 z} - (P_1 + P_2)e^{i\beta_0 z}], & z > a \\ &= (\beta_0/k_x)[P_1 - P_2]e^{-i\beta_0 z}, & z < -a, \end{aligned} \quad (4)$$

$$H_y(z) = -(\omega/k_x c)E_z(z), \quad z > a \quad \text{and} \quad z < -a.$$

Using the expression $S_z \propto \text{Re}(E_x^* H_y)$ for the z component of the Poynting vector above the slab,

$$S_z \propto -4 + |P_1 + P_2|^2, \quad z > a \quad (5)$$

which is the sum of contributions from the incident and reflected waves, and below the slab,

$$S_z \propto -|P_1 - P_2|^2, \quad z < -a \quad (6)$$

for the transmitted wave. Therefore the transmission, reflection, and absorption coefficients are

$$\begin{aligned} T &= \frac{1}{4} |P_1 - P_2|^2, \\ R &= \frac{1}{4} |P_1 + P_2|^2, \\ A &= 1 - T - R = \frac{1}{2}(1 - |P_1|^2) + \frac{1}{2}(1 - |P_2|^2). \end{aligned} \quad (7)$$

These expressions show that T and R involve interference between modes of opposite parity, since P_1 and P_2 are added before being squared. The absorption A , on the other hand, contains no such interference since P_1 and P_2 are squared before being added.

The boundary conditions at the surface of the slab are taken into account by introducing the ratio $g = E_x(z)/\epsilon E_z(z)$, which is continuous across the surface. From Eq. (1) for $E_z^{(1)}(z)$, we find, using $E_x(z) = -(ik_x)^{-1} dE_z(z)/dz$,

$$E_x^{(1)}(z) = (\beta_0/k_x)[e^{-i\beta_0 z} + P_1 e^{i\beta_0 z}], \quad z > a. \quad (8)$$

The value of g just outside the surface, where $\epsilon = 1$, is

$$g_1 = \frac{E_x^{(1)}(z)}{E_z^{(1)}(z)} = \frac{\beta_0 e^{-i\beta_0 a} - P_1 e^{i\beta_0 a}}{k_x e^{-i\beta_0 a} + P_1 e^{i\beta_0 a}} \quad (9)$$

or

$$P_1 = \frac{(\beta_0/k_x) - g_1}{(\beta_0/k_x) + g_1} e^{-2i\beta_0 a}. \quad (10)$$

The subscript 1 always designates the case in which E_z has even parity. Starting with the odd-parity case (2), we find exactly the same relation (10) between P_2 and g_2 .

The fields inside the slab are of the form

$$\begin{aligned} E_z^{(1)}(z) &= e^{\alpha z} + e^{-\alpha z}, \\ E_x^{(1)}(z) &= -(\alpha/ik_x)(e^{\alpha z} - e^{-\alpha z}) \end{aligned} \quad (11)$$

for even parity, or

$$\begin{aligned} E_z^{(2)}(z) &= e^{\alpha z} - e^{-\alpha z}, \\ E_x^{(2)}(z) &= -(\alpha/ik_x)(e^{\alpha z} + e^{-\alpha z}) \end{aligned} \quad (12)$$

for odd parity, where $\alpha = (k_x^2 - \omega^2 \epsilon/c^2)^{1/2}$. g_1 and g_2 can be expressed in terms of these fields just inside the surface:

$$\begin{aligned} g_1 &= E_x^{(1)}(a)/\epsilon E_z^{(1)}(a) = (i\alpha/k_x \epsilon) \tanh \alpha a \\ &= -(i\beta/k_x \epsilon) \tan \beta a \end{aligned} \quad (13)$$

and

$$\begin{aligned} g_2 &= E_x^{(2)}(a)/\epsilon E_z^{(2)}(a) = (i\alpha/k_x \epsilon) \coth \alpha a \\ &= (i\beta/k_x \epsilon) \cot \beta a, \end{aligned} \quad (14)$$

where $\alpha = i\beta$. If we use (13) and (14) in (10), we find

$$\begin{aligned} P_1 &= [(1 + iu_1)/(1 - iu_1)] e^{-2i\beta_0 a}, \\ P_2 &= [(1 + iu_2)/(1 - iu_2)] e^{-2i\beta_0 a}, \end{aligned} \quad (15)$$

where

$$\begin{aligned} u_1 &= (\beta/\beta_0 \epsilon) \tan \beta a, \\ u_2 &= -(\beta/\beta_0 \epsilon) \cot \beta a. \end{aligned} \quad (16)$$

The factors $e^{-2i\beta_0 a}$ in Eq. (15) can be dropped because they cancel when calculating R , T , or A with (7). If we write

$$L_1 = 1 - iu_1 = 1 - (i\beta/\beta_0 \epsilon) \tan \beta a$$

and

$$L_2 = 1 - iu_2 = 1 + (i\beta/\beta_0 \epsilon) \cot \beta a,$$

Eq. (15) becomes

$$\begin{aligned} P_1 &= (2 - L_1)/L_1, \\ P_2 &= (2 - L_2)/L_2. \end{aligned} \quad (17)$$

With the appearance of L_1 and L_2 , Eqs. (7) and (17) exhibit explicitly the relation between the optical properties and the virtual-mode equations. When the frequency is real, (7) and (17) determine the optical properties. If we allow the frequency to become complex, the equations $L_1 = 0$ and $L_2 = 0$ are precisely the virtual-mode equations (2.6) and (2.8) in II.

We can now examine the contribution of the individual virtual modes to the optical absorption. Consider the absorption A_1 due to modes of even parity:

$$A_1 = \frac{1}{2}(1 - |P_1|^2) \\ = (L_1 + L_1^* - 2)/|L_1|^2. \quad (18)$$

The total absorption is $A = A_1 + A_2$, where A_2 , due to modes of odd parity, can be expressed similarly in terms of L_2 . At a fixed value of θ we consider L_1 and u_1 to be functions of the normalized complex frequency $\Omega^c = \omega^c/\omega_T$ and the damping constant γ .⁶ The contribution of an individual mode to A_1 is found by making an expansion of $L_1(\Omega^c, \gamma)$ or $u_1(\Omega^c, \gamma)$ about this mode. Let $\eta = \eta' + i\eta''$ designate the complex frequency of a solution of the virtual-mode equation $L_1 = 0$ with no damping in the dielectric constant ($\gamma = 0$), and let $\rho = \rho' + i\rho''$ designate the frequency of the corresponding solution with damping ($\gamma \neq 0$). That is,

$$L_1(\eta, 0) = 1 - iu_1(\eta, 0) = 0 \quad (19)$$

and

$$L_1(\rho, \gamma) = 1 - iu_1(\rho, \gamma) = 0. \quad (20)$$

If Ω^c is near the virtual-mode frequency ρ , then u_1 can be represented by the linear expansion

$$u_1(\Omega^c, \gamma) = b_1 + b_2\Omega^c + b_3\gamma. \quad (21)$$

From (16) we note that u_1 is real if $\gamma = 0$ and the frequency is real; this implies that b_1 and b_2 are real. Then, using Eqs. (19) and (20) to determine b_1 , b_2 , and b_3 in terms of η and ρ , we can rewrite (21) as

$$u_1 = -(\Omega^c - \rho')/\eta'' + i(\rho'' - \eta'')/\eta''. \quad (22)$$

With the relation $L_1 = 1 - iu_1$ and Eq. (22), Eq. (18) becomes

$$A_1 = 2\eta''\Delta\Omega''/((\Omega - \rho')^2 + (\rho'')^2), \quad (23)$$

where $\Delta\Omega'' = \rho'' - \eta''$ is the shift in the imaginary part of the virtual-mode frequency when the damping factor γ is included in the dielectric constant. The absorption due to an individual mode is therefore a Breit-Wigner resonance peak⁷ centered at ρ' with half-width $|\rho''|$. The relation $\rho'' = \eta'' + \Delta\Omega''$ shows that the total width can be written as the sum of $|\eta''|$, the radiative width due to the flow of energy out of the slab, and $|\Delta\Omega''|$, the change in width due to the presence of damping in the dielectric constant. As pointed out in Sec. 3 of II, the change in width $\Delta\Omega''$ is not a direct measure of γ ; rather, $-\Delta\Omega'' = \frac{1}{2}f'(\Omega, \theta)\gamma$, where $f'(\Omega, \theta)$ is, in general, different from 1.

⁶ When the frequency is allowed to move into the complex plane, we add the superscript c ; thus, ω^c is a complex frequency and $\Omega^c = \omega^c/\omega_T$ is the corresponding dimensionless complex frequency. The expressions for A , T , and R have a physical meaning, however, only for real frequency. Therefore, when we wish to restrict the frequency in these expressions to be real, as in Eqs. (23) and (24), we write it without the superscript, as ω or $\Omega = \omega/\omega_T$.

⁷ J. M. Blatt and V. F. Weisskopf, *Theoretical Nuclear Physics* (John Wiley & Sons, Inc., New York, 1952), Chap. 8.

Equation (23) is not exact, because of the approximations inherent in (21). If γ is not small, terms in Eq. (21) of higher order in γ would be needed. Since the expansion (21) about the complex frequency ρ is used to represent L_1 along the real frequency axis, this procedure becomes inaccurate if ρ is far from the real axis (i.e., if $|\rho''|$ is large). For this reason we expect (23) to be less accurate for wide absorption peaks than for narrow ones. Finally, it was assumed that modes of the same parity are far enough apart that an expansion of $L_1(\Omega^c)$ about a single root is sufficient. One can replace (21) by a polynomial in Ω^c so that the approximation for $L_1(\Omega^c)$ becomes zero at any desired number of roots. This would lead to an expression for the absorption which can reproduce the corresponding number of peaks. However, we shall not carry out this refinement, since we already have an exact expression for the absorption. Particular examples of absorption peaks and their interpretation through Eq. (23) will be discussed later.

Structure in the transmission and reflection coefficients T and R , given by Eq. (7), cannot be associated with the virtual modes as readily as in the case of absorption, because of the interference between P_1 and P_2 . If we use Eqs. (15), (16), and (7), the reflection with no damping ($\gamma = 0$) can be written

$$R = \frac{(\xi^2 - 1)^2}{(\xi^2 - 1)^2 + \xi^2(\cot\beta a + \tan\beta a)^2}, \quad (24)$$

where $\xi = \beta_0\epsilon/\beta$. $R = 0$ when $\xi = 1$, a condition that does not depend on thickness. $\xi = 1$ in two situations: (1) at the frequency $\omega = 2.998\omega_T$ (for LiF) at which $\epsilon = 1$ and $\beta = \beta_0$; (2) when $\omega < \omega_T$ or $\omega > \omega_L$ and the angle of incidence equals Brewster's angle. If, for fixed angle of incidence, the frequency is chosen so that $\beta a = \frac{1}{2}n\pi$ either $\tan\beta a$ or $\cot\beta a = \infty$, and $R = 0$. Since the normal virtual modes occur approximately at frequencies where $\beta a = \frac{1}{2}n\pi$, one would be tempted to conclude that reflectivity minima are associated with virtual modes. Such an identification is incomplete, since we shall see that reflection maxima can also occur.

Suppose, for example, that Ω is near the real part of the complex frequency of a particular virtual mode of type 1, so that L_1 is small. In the normal situation where virtual modes of types 1 and 2 alternate, if Ω is near a virtual mode of type 1, it is about midway between two virtual-mode frequencies of type 2, so that L_2 is large. Then $P_2 \simeq -1$ and Eq. (7) becomes

$$R \simeq \frac{1}{4}|P_1 - 1|^2 \quad (25)$$

or

$$R \simeq \frac{(\Omega - \rho')^2 + (\Delta\Omega'')^2}{(\Omega - \rho')^2 + (\rho'')^2}, \quad (26)$$

where Eq. (22) has been used in going from (25) to (26). R has a minimum at $\Omega = \rho'$, and if $\gamma = 0$ (or $\Delta\Omega'' = 0$), $R = 0$ at the minimum. This result is not quite

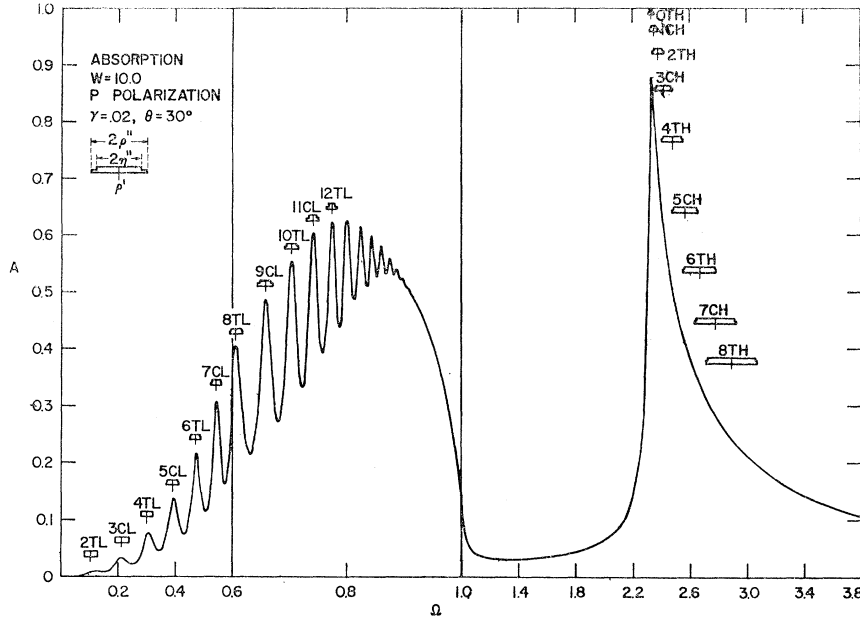


FIG. 1. Absorption as a function of frequency for *P* polarization, thickness $W=10.0$, and angle of incidence $\theta=30^\circ$. There are scale changes in the frequency at $\Omega=0.6$ and 1.0 .

correct because when $\gamma=0$, $R=0$ at a frequency such that $\beta a = \frac{1}{2}n\pi$, not at the virtual-mode frequency η' . This discrepancy appears because L_2 depends on Ω and it is therefore somewhat inaccurate to set P_2 equal to the constant -1 .

There is another interesting case in which, for example, $|u_2| \ll 1$ for Ω near the real part of the frequency of a virtual mode of type 1. Equation (15) then becomes $P_2 \approx 1$, and Eqs. (7) and (22) give

$$R \approx \frac{1}{4} |P_1 + 1|^2 \quad (27)$$

or

$$R \approx \frac{(\eta'')^2}{(\Omega - \rho')^2 + (\rho'')^2} \quad (28)$$

for the reflection due to a virtual mode of type 1. Equation (28) represents a reflection maximum of

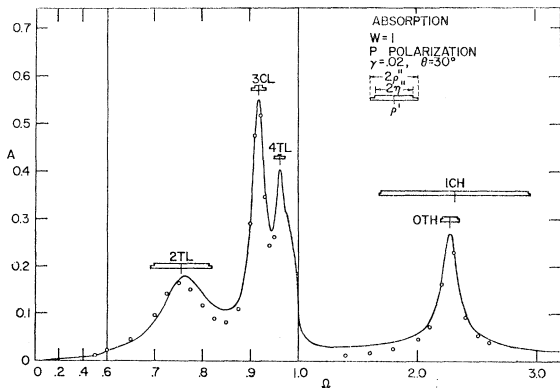


FIG. 2. Absorption as a function of frequency for *P* polarization, thickness $W=1.0$, and angle of incidence $\theta=30^\circ$. There are scale changes in the frequency at $\Omega=0.6$ and 1.0 . The thickness $W=1.0$ corresponds to an actual thickness $L=5.19 \times 10^{-4}$ cm.

width $2|\rho''|$ centered at ρ' , and if $\gamma=0$, $R=1$ at the maximum.

We therefore conclude that a given virtual mode may be associated with either a reflection maximum or minimum, depending on the nature of the interference with modes of opposite parity. From Eq. (7) we see that the expression for T in one case is identical to that for R in the other. Thus, a virtual mode associated with a maximum in R will, in general, give a minimum in T , and vice versa.

S Polarization

The preceding treatment is essentially unchanged for light polarized perpendicular to the plane of incidence. We now have $E_y, H_x,$ and H_z different from zero and $E_x = E_z = H_y = 0$. The Poynting vector is $S_z \propto -\text{Re}(E_y^* H_x)$, and the field ratio which is continuous across the surface of slab is $g = E_y/H_x$ instead of $E_x/\epsilon E_z$. We find, as before, $T = \frac{1}{4} |P_1 - P_2|^2$, $R = \frac{1}{4} |P_1 + P_2|^2$, $A = \frac{1}{2} (1 - |P_1|^2) + \frac{1}{2} (1 - |P_2|^2)$, where $P_1 = (1 + iu_1)/(1 - iu_1)$ and $P_2 = (1 + iu_2)/(1 - iu_2)$. The subscripts 1 and 2 refer, respectively, to fields E_y of even and odd parity. The essential change is that instead of Eq. (16), we have

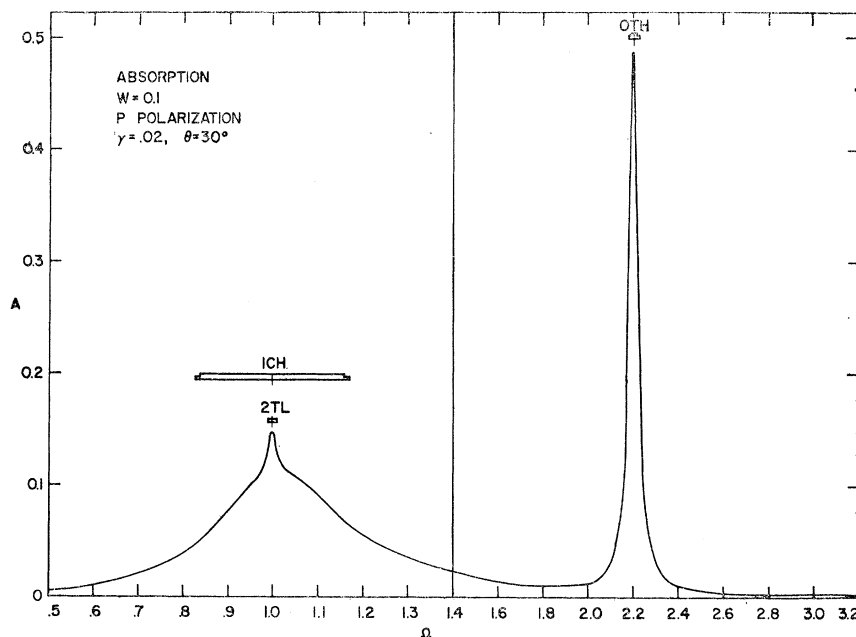
$$\begin{aligned} u_1 &= (\beta/\beta_0) \tan \beta a, \\ u_2 &= -(\beta/\beta_0) \cot \beta a. \end{aligned} \quad (29)$$

We can again write $P_1 = (2 - L_1)/L_1$ and $P_2 = (2 - L_2)/L_2$, in which $L_1 = 0$ and $L_2 = 0$, for complex frequency, are the virtual-mode equations (2.10) and (2.11) of II:

$$\begin{aligned} L_1 &= 1 - i(\beta/\beta_0) \tan \beta a = 0, \\ L_2 &= 1 + i(\beta/\beta_0) \cot \beta a = 0. \end{aligned}$$

Therefore, the optical properties for *S* polarization can again be associated with the virtual modes. The

FIG. 3. Absorption as a function of frequency for P polarization, thickness $W=0.1$, and angle of incidence $\theta=30^\circ$. There is a scale change in the frequency at $\Omega=1.4$.

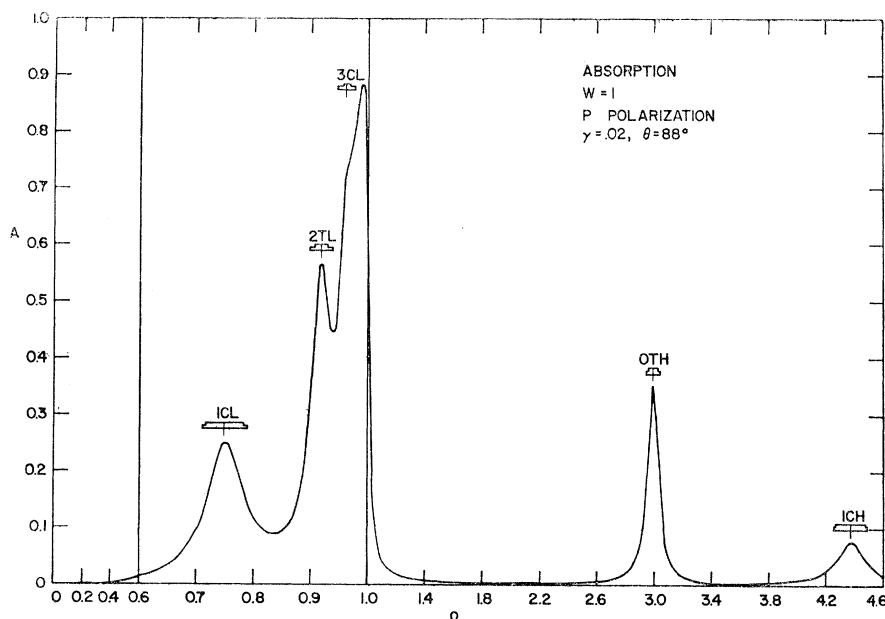


differences in optical properties for the two directions of polarization arise from differences in the virtual modes, which are due to the missing ϵ in the combination $\xi'=\beta/\beta_0$ for S polarization, as compared with $\xi=\beta/\beta_0\epsilon$ for P polarization. This means that there is no Brewster's angle for S polarization, and effects which were associated with this angle disappear. For example, referring to Eq. (24), where $\xi'=\beta/\beta_0$ appears instead of ξ , the condition $\xi'=1$ for which $R=0$ with no damping can no longer occur at various frequencies at the Brewster's angle, but occurs only at $\omega=2.998\omega_T$ (for LiF).

III. COMPARISON WITH EXACT CALCULATION

The foregoing results will now be illustrated by exact calculations of A , T , and R for a LiF slab of various thicknesses. As in the virtual-mode calculations of Paper II, we have used a frequency-independent damping constant $\gamma=0.02$. Figures 1, 2, and 3 show the absorption A for P polarization as a function of the normalized frequency Ω for thicknesses $W=10.0$, 1.0 , and 0.1 , at a fixed angle of incidence, $\theta=30^\circ$. In Fig. 4 the thickness is $W=1.0$ and the angle is $\theta=88^\circ$. The central point to be noted in these figures is that the

FIG. 4. Absorption as a function of frequency for P polarization, thickness $W=1.0$, and angle of incidence $\theta=88^\circ$. There are scale changes in the frequency at $\Omega=0.6$ and 1.0 .



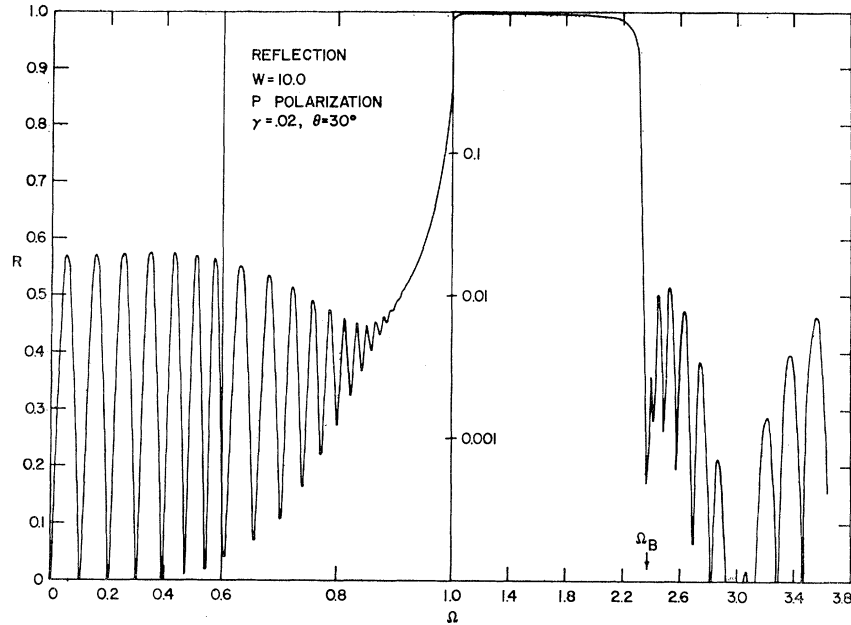


FIG. 5. Reflection as a function of frequency for *P* polarization, thickness $W=10.0$, and angle of incidence $\theta=30^\circ$. There are scale changes in the frequency at $\Omega=0.6$ and 1.0 , and a vertical scale change at $\Omega=1.0$.

absorption peaks can be associated with the virtual modes as calculated in II. Thus, each peak is labeled by the number of the mode with which it is associated (e.g., $2TL$, $3CL$, ...). The double bar above each peak illustrates the center frequency ρ' of the virtual mode, its radiative width $|2\eta''|$ calculated with $\gamma=0$, and its total width $|2\rho''|$ calculated with $\gamma=0.02$.

The absorption peaks shown for $W=10.0$ in Fig. 1 are resolved only for frequencies $\Omega < 1$. The total width $|2\rho''|$ of the first peaks is almost entirely radiative [i.e., the function $f'(\Omega, \theta)$ discussed in II is small at low frequencies]. As Ω increases, the radiative width decreases, but the total width does not become smaller

than $2(\gamma/2)=0.02$. Thus when $0.9 < \Omega < 1.0$, the spacing between modes is smaller than their width, and the absorption peaks merge. The large peak starting at about $\Omega=2.3$ and extending to higher frequencies is derived from all the high-frequency modes. Since the widths of these modes are greater than the separation, they are unresolved. The mode OTH , which is responsible for the maximum at $\Omega=2.330$, is at a frequency somewhat higher than $\Omega_L=2.197$, the usual longitudinal optical (LO) frequency, because $\theta \neq 0$. The absorption due to this mode disappears at normal incidence because $\eta'' \rightarrow 0$ as $\theta \rightarrow 0$ [see Eq. (23)].

In a slab of intermediate thickness $W=1$ (Fig. 2),

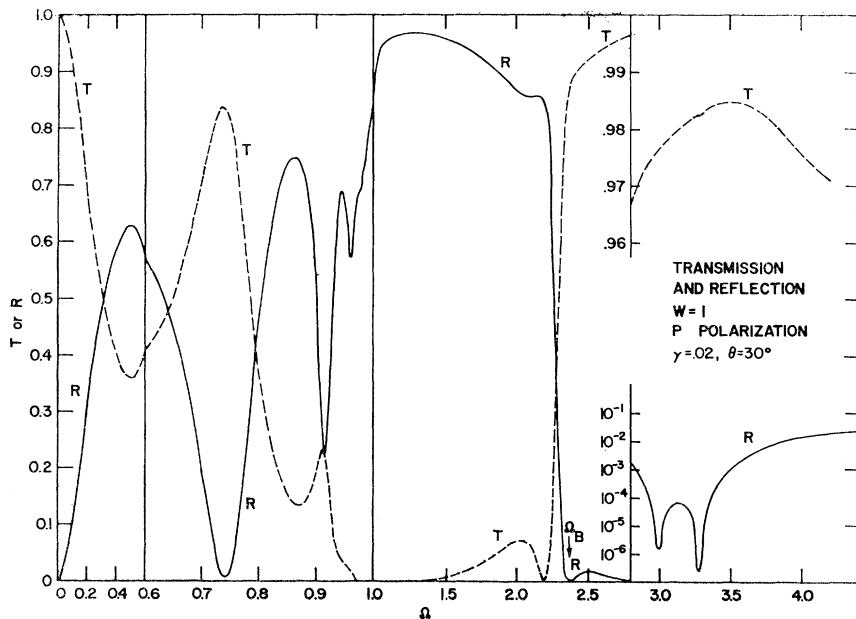
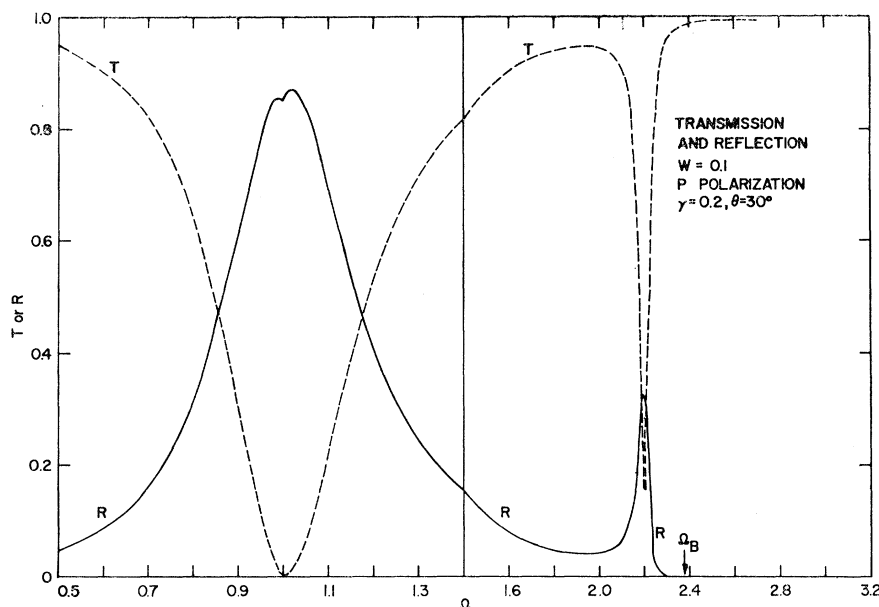


FIG. 6. Transmission and reflection as a function of frequency for *P* polarization, thickness $W=1.0$, and angle of incidence $\theta=30^\circ$. There are scale changes in the frequency at $\Omega=0.6$ and 1.0 , and a vertical scale change at $\Omega=2.8$.

FIG. 7. Transmission and reflection as a function of frequency for P polarization, thickness $W=0.1$, and angle of incidence $\theta=30^\circ$. There is a scale change in the frequency at $\Omega=1.4$.



most of the low-frequency modes have moved close to the transverse optical (TO) frequency, and only the first three peaks are clearly resolved. All except two of the high-frequency modes are off the scale at the right, the $2TH$ mode occurring at $\Omega=3.430$. The widths of the $0TH$ and $1CH$ modes have increased, and the relatively narrow $0TH$ peak is superimposed on the very broad $1CH$ peak. The $0TH$ peak is now at $\Omega=2.268$, somewhat closer to the LO frequency 2.197 than in the case of the thicker slab.

In Fig. 3, for $W=0.1$, only three modes $1CH$, $2TL$, and $0TH$ are shown. The sharp peak just below $\Omega=1$ is due primarily to the $2TL$ mode; the higher modes $3CL$, $4TL$, \dots , which are not shown, contribute only slightly to this peak and lie very close to $\Omega=1$. The sharp peak is superimposed on a broad peak due to the $1CH$ mode. It has already been noted in II that this mode behaves in a very strange manner. As the thickness of the slab becomes less than $W=1$, the $1CH$ mode in Fig. 2 becomes even broader and starts to move below the LO frequency. For $W \lesssim 0.3$ it moves below the TO frequency and its width starts to decrease. The $0TH$ peak in Fig. 3, which broadened as W changed from 10 to 1, has started to become narrow again, and has moved to $\Omega=2.199$, very close to $\Omega_L=2.197$.

As the thickness becomes smaller than $W=0.1$, the $1CH$ and $0TH$ peaks continue to become narrower and the composite peak $2TL$, $3CL$, \dots disappears entirely. For $W=0.01$, for example, the total width of the $1CH$ mode is $2|\rho''|=0.0518$ and for the $0TH$ mode, $2|\rho''|=0.0228$. Although the width in the limit $W \rightarrow 0$ is $2|\rho''| \rightarrow \gamma=0.02$, one must go to a very thin crystal in order that the radiative contribution to the width of the $1CH$ mode be negligible compared to γ . In a calculation by Vredevoe⁸ of the third-order anharmonic con-

tribution to the width of the peak at the transverse optical frequency in NaCl, a comparison was made with the measured width of the absorption peak in a film of thickness 0.17μ at normal incidence.⁹ Using parameters for NaCl in Eq. (2.33) of II, we find that the radiative width of the $1CH$ mode is $2|\eta''|=0.014$, which is not negligible compared to the measured total width $2|\rho''|=0.081$. The correct damping constant to be compared with theory is, therefore, $\gamma=2|\rho''|-2|\eta''|=0.067$. Although Vredevoe's theoretical calculation of γ was not sufficiently accurate to make this correction important, this example shows that one must proceed with caution when inferring the value of γ from the measured width of an absorption peak.

The change in absorption when going from $\theta=30^\circ$ to $\theta=88^\circ$ is seen by comparing Figs. 2 and 4. Each low-frequency mode for 88° is approximately at the frequency of the next higher mode for 30° , and the first mode for 88° , $1CL$, does not appear at all for 30° . The first high-frequency mode, $0TH$, moves to $\Omega=2.998$ ($\epsilon=1$) and the $1CH$ mode moves to a still higher frequency. Since the radiative width becomes zero at $\theta=90^\circ$, the modes at 88° are relatively narrow.

We can compare the exact calculation of the absorption with the approximation (23) for the absorption due to a single mode. When several modes contribute to the absorption at a given frequency, we shall simply add the contributions from the various modes. Although this procedure is not quite correct, since modes of the same parity do not contribute additively, it does not lead to serious errors in cases for which modes of the same parity do not overlap too much (the high-frequency absorption for $W=10$, for example, consists of overlapping modes and cannot be treated in this way). The circled points in Fig. 2 show the result of such a calcula-

⁸ L. Vredevoe, Phys. Rev. **140**, A930 (1965).

⁹ R. Barnes and M. Czerny, Z. Physik **72**, 447 (1931).

tion, using Eq. (23). In the range $0.5 < \Omega < 0.95$ we have taken the sum of the absorption due to the three modes $2TL$, $3CL$, and $4TL$, while the $0TH$ and $1CH$ modes have been used for $1.4 < \Omega < 2.6$. The absorption found in this way near the $2TL$ mode does not agree well with the exact curve; the actual peak lies on the high-frequency side of the virtual-mode peak, and is larger. The agreement is much better near the $3CL$ mode (the inclusion of modes higher than $4TL$ would have raised the points near $\Omega=0.95$). The contribution from the $0TH$ mode agrees well with the true absorption, while the superimposed $1CH$ absorption does not agree so well, as can be seen from the discrepancy at $\Omega=1.4$ to 2.0 . We have pointed out in Sec. II that the disagreement for the wide peaks is to be expected. Conversely, narrow absorption peaks, especially isolated ones such as the $0TH$ peak for $W=0.1$, $\theta=30^\circ$ or $W=1.0$, $\theta=88^\circ$ are represented very accurately by Eq. (23).

It should be pointed out why the $0CL$ mode is missing in Figs. 1, 2, and 3. At $\theta=30^\circ$, this mode has a frequency with real part zero and negative imaginary part. When γ is added, the magnitude of the imaginary part decreases instead of increases, as more normal modes do. Therefore, $\Delta\Omega'' > 0$, and since $\eta'' < 0$, the absorption is negative, according to (23). This unique result actually is necessary, as the negative absorption in principle cancels the positive absorption due to the other modes at $\Omega=0$, leading to the required result $A \rightarrow 0$ as $\Omega \rightarrow 0$.¹⁰

Reflection and Transmission

Figures 5, 6, and 7 show reflection and/or transmission coefficients at $\theta=30^\circ$ with P polarization for three thicknesses: $W=10.0$, 1.0 , and 0.1 . We have shown that R and T cannot readily be interpreted in terms of the virtual modes because of the interference between modes of opposite parity.

These figures show the two thickness-independent reflection minima at $\Omega=2.998$ for which $\epsilon=1$, and at $\Omega=2.373$ (marked Ω_B on the figures) for which the Brewster's angle condition at $\theta=30^\circ$ is satisfied. For $W=10.0$ and 1.0 there are the "normal" reflection minima at frequencies satisfying $\beta a = \frac{1}{2}n\pi$. These can be associated approximately with virtual modes, according to Eq. (26). For $W=0.1$, on the other hand, there is no longer a minimum, but a broad reflection maximum at $\Omega \simeq 1$ associated with the $1CH$ mode, and another maximum at $\Omega \simeq 2.197$, with the $0TH$ mode. Thus, (28) is the appropriate expression for the reflection in this case. The small drop in reflection near the top of the broad peak at $\Omega \simeq 1$ is a "normal" effect due to the remaining virtual modes clustered just below $\Omega=1$.

¹⁰ The complete cancellation does not actually take place if (23) is used for the absorption due to each mode and the contributions from the different modes are added. This is due to the approximations in (23) and the fact that the assumption of additivity is somewhat inaccurate.

As the thickness of the slab becomes still smaller than $W=0.1$, the radiative width of the reflection maximum near ω_T due to the $1CH$ mode continues to decrease while its frequency approaches ω_T , and the effect of the other modes near ω_T disappears. The sizes and widths of the reflection maxima (or transmission minima) at ω_T and ω_L , which are the dominant features of the optical properties of a very thin slab, are therefore explained completely in terms of the $1CH$ and $0TH$ modes.

There is a qualitative explanation in terms of virtual modes for the fact that R is large in the range $1 < \Omega < 2.2$ for a thicker slab ($W=10.0$ or 1.0) and is small, at least in the higher part of this range, for the thin slab ($W=0.1$). It can be shown that in a thick slab, $u_1 \simeq u_2$, and, therefore, from (5) and (7), $P_1 \simeq P_2$ or $R \simeq 1$. In a thin slab, however, $|u_1| \ll 1$ and $|u_2| \gg 1$, giving $P_1 \simeq 1$, $P_2 \simeq -1$, or $R \simeq 0$. The equality of u_1 and u_2 for a thick slab, in terms of the virtual-mode distribution, is a result of the alternation of nearby modes of opposite parity for both $\Omega < 1$ and $\Omega > 2.2$. The two kinds of modes therefore collectively make about the same contribution to u_1 and u_2 , respectively, in the region $1 < \Omega < 2.2$. In a thin crystal, the contributions to u_1 in this region from the tangent modes just below $\Omega=1$ and the $0TH$ mode at $\Omega=2.2$ are of opposite sign and must almost cancel, making $|u_1|$ small. No similar cancellation occurs for the cotangent modes because the $1CH$ mode, which was paired with the $0TH$ mode in a thick crystal, moved to a low frequency as W decreased from 0.7 to 0.3 . Therefore, in a thin slab the $1CH$ and other low-frequency cotangent modes near $\Omega=1$ contribute additively to u_2 , making $|u_2| > 1$. We conclude that the transition from large R to small R for $1 < \Omega < 2.2$ as W decreases is associated with the passage of the $1CH$ mode through this region.

Crystal Slab on a Conducting Substrate

Expressions for the optical properties of an ionic crystal slab of thickness $\frac{1}{2}W$ on a perfectly conducting substrate can be derived by noting that the boundary conditions $E_x = E_y = 0$ at the conductor are satisfied at the center of a slab of thickness W in free space by virtual modes of odd parity in E_x or E_y . For P polarization the fields of odd parity in E_x are of even parity in E_z , as in Eq. (1). Therefore from Eq. (1) we immediately find $R = |P_1|^2$ and $A = 1 - |P_1|^2$. Therefore since only a single parity is involved, neither R nor A contains interference between modes of opposite parity. Similarly we find $R = |P_2|^2$ and $A = 1 - |P_2|^2$ for S polarization.

ACKNOWLEDGMENT

The authors wish to acknowledge stimulating discussion with and helpful comments from Professor David Lynch.